Efficient Carrier Multiplication in Colloidal CuInSe2 Nanocrystals

ARTICLE *in* JOURNAL OF PHYSICAL CHEMISTRY LETTERS · SEPTEMBER 2014

Impact Factor: 7.46 · DOI: 10.1021/jz501640f

3 AUTHORS, INCLUDING:

C. Jackson Stolle
University of Texas at Austin
12 PUBLICATIONS **235** CITATIONS

THE JOURNAL OF PHYSICAL CHEMISTRY Letters

Letter

pubs.acs.org/JPCL

Efficient Carrier Multiplication in Colloidal $CuInSe_2$ Nanocrystals

C. Jackson Stolle,[†] Richard D. Schaller,[‡,§] and Brian A. Korgel*[,†]

[†]McKetta Department of Chemical Engineering, Texas Materials Institute, Center for Nano- and Molecular Science and Technology, The University of Texas at Austin, Austin, Texas 78712, United States

[‡]Department of Chemistry, Northwestern University, Evanston, Illinois 60208, United States

[§]Center for Nanoscale Materials, Argonne National Laboratories, Argonne, Illinois 60439, United States

Supporting Information

ABSTRACT: Transient absorption spectroscopy (TAS) was used to study carrier multiplication (CM) (also called multiexciton generation (MEG)) in solvent-dispersed colloidal $CuInSe_2$ nanocrystals with diameters as small as 4.5 nm. Size-dependent carrier cooling rates, absorption cross sections, and Auger lifetimes were also determined. The energy threshold for CM in the $CuInSe_2$ nanocrystals was found to be 2.4 ± 0.2 times the nanocrystal energy gap (*Eg*) and the CM efficiency was 36 ± 6% per unit *Eg*. This is similar to other types of nanocrystal quantum dot materials.

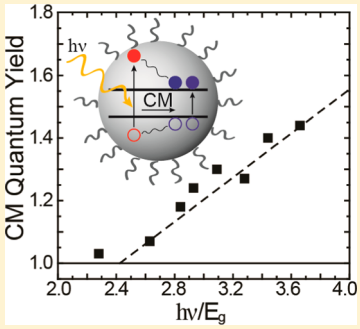

SECTION: Physical Processes in Nanomaterials and Nanostructures

The absorption of a photon by a semiconductor typically leads to the formation of a single electron–hole pair, and the photon energy exceeding the band gap is lost as heat. However, an absorbed photon can also create more than one electron–hole pair, or exciton, if the photon provides enough energy. In bulk semiconductors, multiple exciton generation (MEG)—or carrier multiplication (CM)—typically requires photons with at least four times the band gap energy.[1] Quantum dots on the other hand, can exhibit especially efficient CM and the CM efficiency tends to increase with decreasing quantum dot size.[2−4] The mechanism of multiexciton formation has been the subject of several experimental and theoretical studies.[5−8] CM has been observed spectroscopically in a variety of nanocrystals, including Si, PbS, PbSe, PbTe, CdSe, Ag_2S, InP, InAs, and $CuInSe_2$ with photon energies nearing two times the optical gap.[9−17] Photovoltaic devices of PbSe[18] and $CuInSe_2$[17] nanocrystals have also been made showing peak external quantum efficiencies exceeding 100% in the wavelength range where CM occurs, indicating that photogenerated multiexcitons can also be extracted. In the case of the $CuInSe_2$ nanocrystal films used to make PV devices with >100% EQE, transient absorption spectroscopy (TAS) measurements confirmed spectroscopically that CM indeed occurred in those $CuInSe_2$ nanocrystal films.[17] In this Letter, we report a more extensive set of size-dependent TAS measurements of $CuInSe_2$ nanocrystal dispersions to determine the CM efficiency, the energy threshold for CM, the carrier cooling rates, absorption cross sections, and Auger lifetimes of $CuInSe_2$ nanocrystals. The $CuInSe_2$ nanocrystals had slightly lower CM threshold energy, longer Auger lifetimes, and similar CM efficiency as compared to spherical PbSe nanocrystal quantum dots.

TAS measurements were performed on $CuInSe_2$ nanocrystals of three different sizes synthesized using the methods of Panthani et al.[19] (see Supporting Information for Experimental Details). Figure 1 shows transmission electron microscopy (TEM) and UV–vis absorbance spectra of the nanocrystals, which have average diameters of 4.5 ± 0.8, 6.2 ± 1.5, and 9.2 ± 3.2 nm. The optical absorption edge shifts to higher energy with decreasing size due to quantum confinement. There are no exciton peaks in the spectra for these relatively large sizes. Absorbance spectra of smaller nanocrystals with exciton peaks are shown in the Supporting Information (Figure S1). These smaller sizes were not studied by TAS because of the relatively high photon energies required to produce multiple excitons. X-ray diffraction (XRD) showed that the nanocrystals are composed of the compositionally ordered chalcopyrite $CuInSe_2$ crystal phase (see Supporting Information Figure S2).

Figure 2 shows TA bleach spectra of three different sizes of $CuInSe_2$ nanocrystals dispersed in toluene obtained using an 800 nm pump laser and a white light probe beam. All TAS measurements were carried out with magnetic stirring to ensure that photocharging did not influence the detected signal (see Supporting Information for Experimental Details).[21] Peaks in the TA bleach spectra appear at 1170 nm (1.06 eV), 1050 nm (1.18 eV), and 910 nm (1.36 eV) for nanocrystals with average diameters of 9.2, 6.2, and 4.5 nm, respectively, corresponding to

Received: August 4, 2014
Accepted: August 27, 2014

   dx.doi.org/10.1021/jz501640f | *J. Phys. Chem. Lett.* 2014, 5, 3169−3174

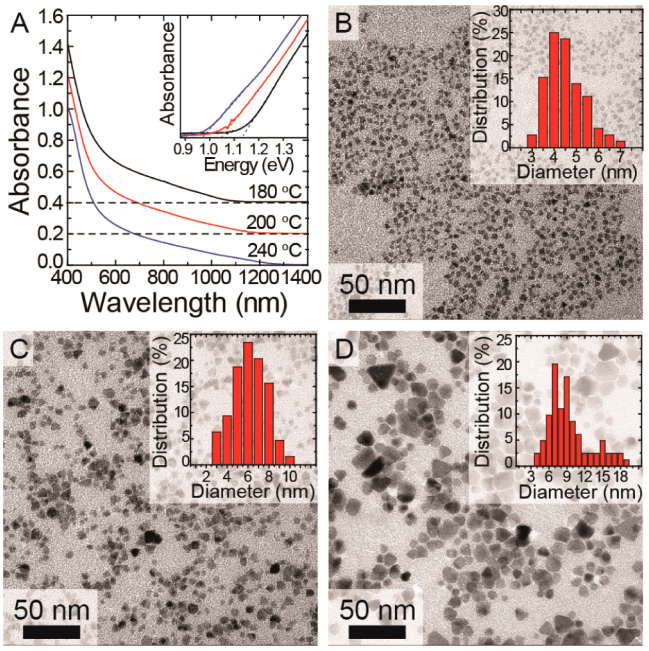

Figure 1. $CuInSe_2$ nanocrystals studied by TAS: (A) optical absorbance spectra and (B–D) TEM images. (A) Absorbance spectra were measured at room temperature for nanocrystals dispersed in toluene. Spectra are offset by 0.2 O.D. for clarity. The temperatures noted in (A) correspond to the synthesis temperatures used to make the samples with corresponding TEM images in (B) 180 °C, (C) 200 °C, and (D) 240 °C. The insets of (B–D) are size histograms obtained from the TEM images average diameters of (B) 4.5 ± 0.8 nm, (C) 6.2 ± 1.5 nm and (D) 9.2 ± 3.2 nm. The absorption edges determined in the inset of (A) are 0.98 eV (240 °C), 1.05 eV (200 °C), and 1.14 eV (180 °C).[20]

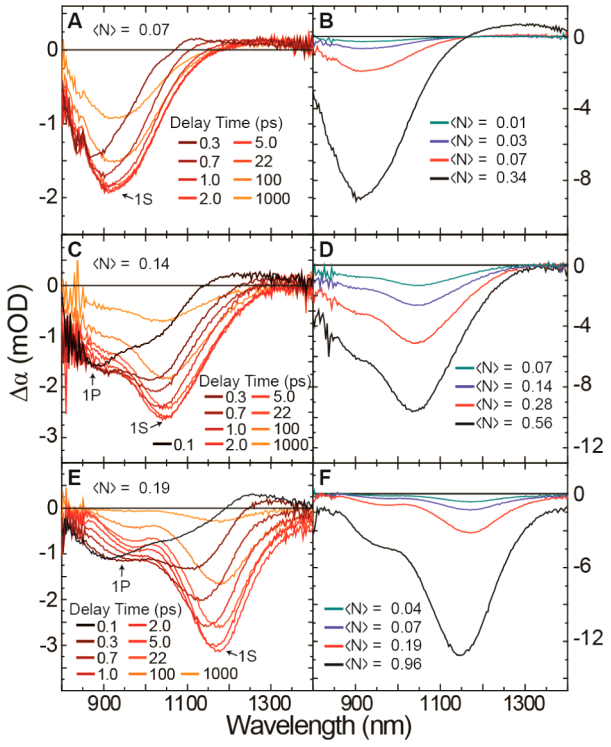

Figure 2. $CuInSe_2$ nanocrystal transient absorption spectra (TAS) acquired with 800 nm pump wavelength. Samples with three different average diameters were measured: (A, B) 4.5 ± 0.8 nm, (C, D) 6.2 ± 1.5 nm, and (E, F) 9.2 ± 3.2 nm. (A, C, E) show the evolution of the TA bleach spectra as a function of delay time (spectra with 0.1 ps delay time are shown in black) and (B, D, F) show TA spectra of each sample after 2.5 ps delay time with varying average number of photons absorbed per nanocrystal, $\langle N \rangle$. $\langle N \rangle$ was varied by changing the pump fluence, j_p (number of photons/cm^2): $\langle N \rangle = \sigma j_p$, where σ is the absorption cross section of each nanocrystal sample (cm^2) (see Figure 4).

to the 1S absorption edge. In the very early time regime (<2 ps), the TA peak appears initially at slightly shorter wavelength than the 1S feature because of the presence of hot carriers. As the hot carriers relax to the conduction and valence band minima, the bleach peak shifts to slightly longer wavelength.[22] After 2.5 ps of delay, the wavelength of the 1S-related peaks in the TA spectra are largely unaffected by delay time or pump fluence, as shown in Figure 2B, D, and F.

The carrier cooling rates were calculated from the intraband cooling times determined from the evolution of the TA peak absorption at relatively short delay times (<5 ps) in Figure 3A.[23] Figure 3B shows the carrier cooling rates plotted as a function of nanocrystal size. The carrier cooling rate increases as the nanocrystals become smaller, and there is a linear relationship between particle volume and carrier cooling rate, which is consistent with experimental results and theory for other semiconductor nanocrystals.[22−24]

Figure 4 shows the absorption cross sections calculated from TAS. In Figure 4A and B, the bleached absorption signals measured after 1 ns delay time using different pump fluences of 400 and 800 nm light are shown. After 1 ns, only single excitons are present in the nanocrystals (i.e., the biexciton lifetime is much shorter than 1 ns). The increase in the absorption bleach signal with increasing pump fluence (or photon flux j_p) at long time delays depends on the absorption cross section, σ;[25]

$$-\Delta\alpha \propto (1 - e^{-\sigma j_p}) \quad (1)$$

As shown in Figure 4, the bleached absorption signal increases linearly with increasing pump fluence and then saturates. The ratios of the (400 and 800 nm) absorption cross sections in Figure 4C are consistent with the absorbance spectra in Figure 1 (8:1 for all three nanocrystal sizes by TAS compared to 7:1 from the absorbance spectra). These absorption cross sections are comparable to those of PbSe nanocrystals with similar size.[16]

Figure 5 shows the TA kinetics of three different sizes of $CuInSe_2$ nanocrystals using two pump wavelengths (400 and 800 nm). A single absorbed 800 nm photon cannot generate more than one exciton, so the TA kinetics at low fluence (normalized at 1 ns) represent the single exciton decay. Multiple excitons are photoexcited with 800 nm light by increasing the pump fluence to induce multiphoton absorption.[10] When multiphoton absorption occurs, the normalized TA kinetics show a higher intensity early time signal with a biexponential decay and two carrier relaxation processes come into play: (1) a fast Auger recombination process (the process inverse to CM) and (2) a much longer lived single exciton signal. The biexciton (Auger) lifetimes were determined by subtracting the normalized single exciton baseline TA kinetics (low fluence, 800 nm pump wavelength) and fitting the signal to a single exponential function (see Supporting Information Figure S3). The Auger lifetimes are plotted in Figure 6A as a function of particle volume. The biexciton lifetime scales linearly with particle volume, consistent with literature reports.[26]

dx.doi.org/10.1021/jz501640f | J. Phys. Chem. Lett. 2014, 5, 3169−3174

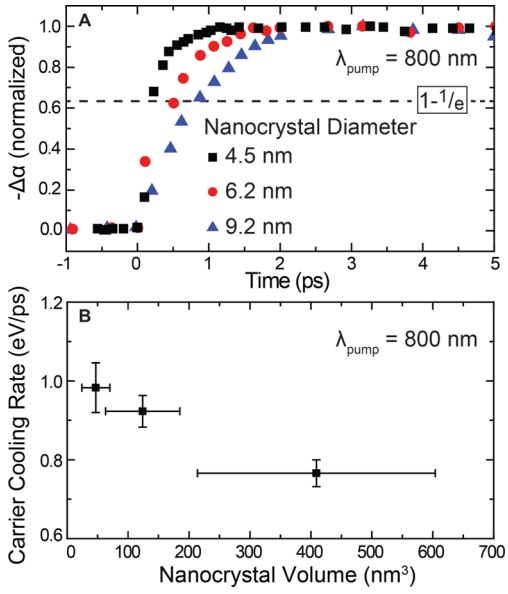

Figure 3. Carrier cooling rates. (A) Early−time (<5 ps) TA kinetics for each nanocrystal sample at 800 nm pump wavelength (black squares, 4.5 nm nanocrystals; red circles, 6.2 nm nanocrystals; blue triangles, 9.2 nm nanocrystals). The TA kinetics are examined at the location of the absorption bleach maximum for each sample (910 nm for the 4.5 nm diameter nanocrystals, 1050 nm for the 6.2 nm nanocrystals, and 1170 nm for the 9.2 nm nanocrystals). The maximum bleach signals are normalized to one. To calculate the carrier cooling rate, the characteristic cooling times were taken as the delay time when the normalized TA bleach increased from zero to $1 - (1/e)$ (dashed line).[23] (B) Carrier cooling rates versus nanocrystal volume measured using 800 nm pump wavelength. Carrier cooling rates were calculated from the difference in energy between the 800 nm pump energy and the nanocrystal optical gap (taken as the peak of the TA bleach) divided by the carrier cooling time. The nanocrystal volume was determined from the average diameter assuming spherical shape. The error bars shown for the carrier cooling rate represent the standard deviation obtained from four measurements using different pump fluence. The error bars for nanocrystal volume correspond to the standard deviation of particle size distribution.

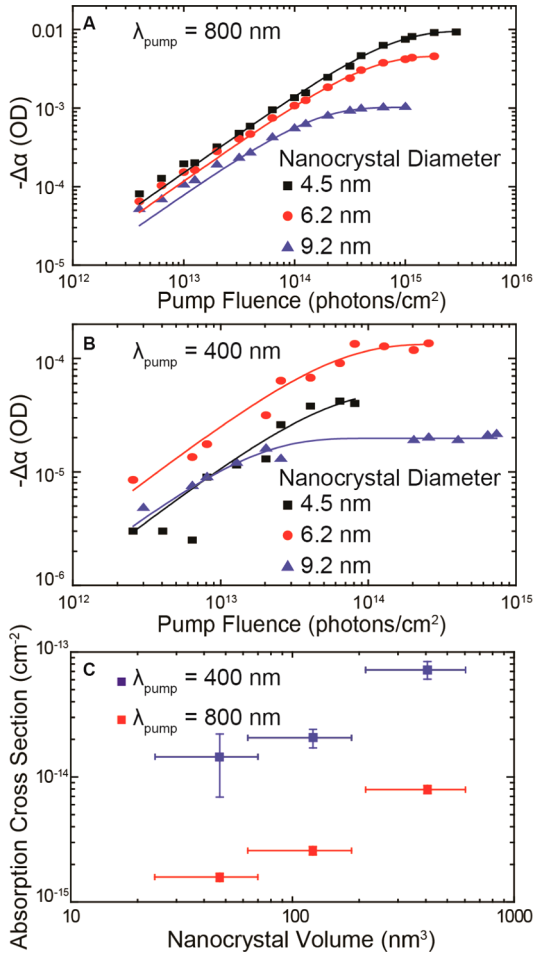

Figure 4. Absorption cross section. Transient absorption signal at long delay time (1000 ps) for each nanocrystal sample (4.5 nm, black squares; 6.2 nm, red circles; 9.2 nm, blue triangles) as a function of pump fluence for (A) 800 nm pump wavelength and (B) 400 nm pump wavelength. (C) Absorption cross section plotted against particle volume for both (blue) 400 nm pump wavelength and (red) 800 nm pump wavelength. The absorption cross section is calculated by fitting the data in A and B to eq 1. The error bars for absorption cross section correspond to error in the fit of the data to eq 1.

The TA kinetics measured using 800 nm pump light provide the single exciton TA kinetics baseline (using low fluence pump) and the biexciton Auger recombination kinetics (using high fluence pump) for comparison to the TA kinetics using 400 nm pump light. Figure 5b shows the TA kinetics of the 4.5 nm diameter nanocrystals measured using 400 and 800 nm pump light. The signals overlap, indicating that the TA decay does not result from hot carrier cooling and that the energy of the 400 nm photons (equal to $2.28E_g$) lies below the energy threshold for CM. The TA kinetics for the larger nanocrystals (6.2 and 9.2 nm) obtained using 400 nm pump light (Figure 4D and F), show much faster kinetics at early times, indicative of Auger recombination. The average number of photons absorbed per nanocrystal is low under these conditions (0.13 and 0.2 photons per nanocrystal for the 6.2 and 9.2 nm particles, respectively), and therefore, the observed Auger recombination is attributed to carrier multiplication.[10]

To determine the CM quantum yield, TAS was performed using a range of low pump fluences where the TA signal is independent of the pump fluence (see Supporting Information Figure S4). The CM quantum yield was measured using pump wavelengths of 800, 400, 340, and 320 nm and taking the ratio of the average TA signal at high energy pump (either 400, 340, or 320 nm) to the average single exciton TA signal (800 nm pump wavelength). Figure 6B shows the CM quantum yield measured as a function of photon energy relative to the nanocrystal optical gap. A weighted fit of the data gives a straight line with a slope corresponding to the CM efficiency (36 ± 6%). The energy where the line intersects QY = 1 is the CM threshold $(2.4 \pm 0.2)E_g$.[1] This means that an extra 0.36 excitons are generated per absorbed photon (on average) for each band gap multiple of energy that the incident photon energy is increased above the CM threshold. These data fit well with our previous transient absorption measurements on $CuInSe_2$ nanocrystal thin films, which showed a CM QY of ~1.25 at photon energies of $3.1E_g$.[17]

Multiexciton single junction solar cells require a light-absorbing layer with a combination of high CM efficiency, low CM threshold, long Auger lifetimes, and an optimal band gap. The CM efficiency of the $CuInSe_2$ nanocrystals is comparable to PbSe (36% vs 40%), which is the only other material to demonstrate EQE values exceeding 100% in PV devices.[17,18,27] The CM threshold for PbSe is $3E_g$.[27] The lower CM threshold

dx.doi.org/10.1021/jz501640f | J. Phys. Chem. Lett. 2014, 5, 3169−3174

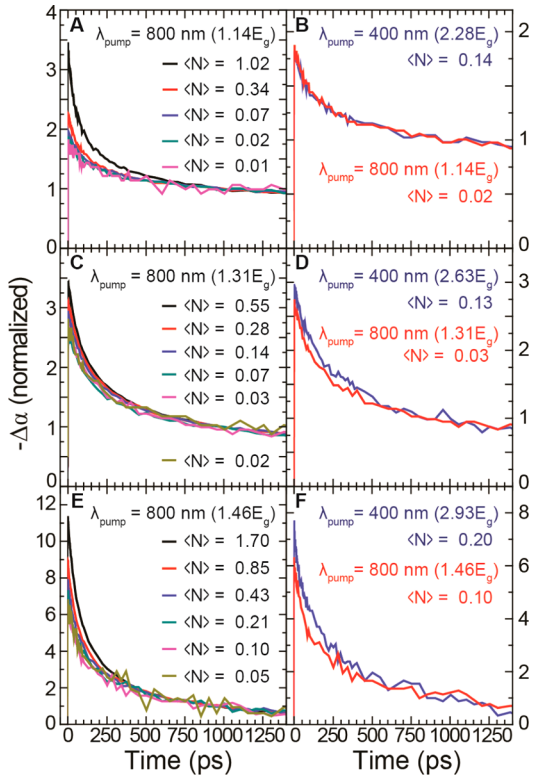

Figure 5. Transient absorption kinetics of (A, B) 4.5 ± 0.8 nm nanocrystals, (C, D) 6.2 ± 1.5 nm nanocrystals, and (E, F) 9.2 ± 3.2 nm diameter $CuInSe_2$ nanocrystals measured using two different pump wavelengths of 400 and 800 nm. All curves are normalized at long delay times (1 ns) where only single excitons are present in the nanocrystals. Transient absorption kinetics taken with a low pump fluence at 400 and 800 nm pump wavelength for (B) 4.5 nm nanocrystals, (D) 6.2 nm nanocrystals, and (F) 9.2 nm nanocrystals, where the kinetics measured at 400 nm are shown in blue and kinetic measured at 800 nm are shown in red. The kinetics are taken at the peak in the absorption bleach for each sample (910 nm for the 4.5 nm particles, 1050 nm for the 6.2 nm particles, and 1170 nm for the 9.2 nm particles).

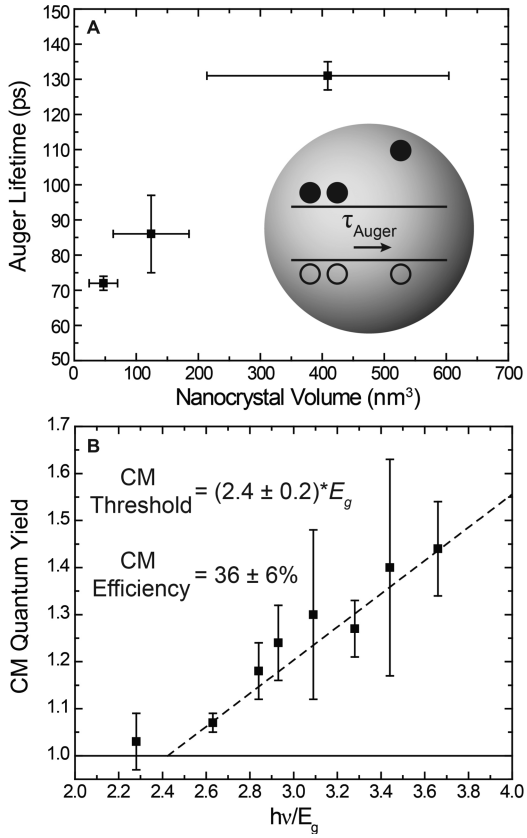

Figure 6. Auger lifetimes and CM quantum yield. (A) Biexciton lifetimes plotted against particle volume for the 4.5 ± 0.8, 6.2 ± 1.5, and 9.2 ± 3.2 nm diameter $CuInSe_2$ nanocrystals. The error bars for nanocrystal volume correspond to the standard deviation of nanocrystal sizes within each sample. The error bars for biexciton lifetime correspond to error in the single exponential fit in Supporting Information Figure S3. (B) CM quantum yield plotted as a function of pump energy (relative to the nanocrystal band gap energy). Data were collected for 4.5, 6.2, and 9.2 nm diameter nanocrystals using pump wavelengths of 400, 340, and 320 nm. The data are fit to a straight line, excluding the data point at $2.28E_g$, which is below the CM threshold. The intersection of the lines QY = 0 and the fit line is defined as the CM threshold ($(2.4 \pm 0.2)E_g$) and the slope of the fit line times 100% is defined as the CM efficiency (36 ± 6%). Error bars for the measured CM quantum yield correspond to the standard deviation of quantum yields measured for a range of pump fluences (see Supporting Information Figure S4).

for $CuInSe_2$ nanocrystals of $2.4E_g$ provides for the possibility of slight gains in the device efficiency. For example, the maximum efficiency of a multiexciton device, assuming 100% CM QY, could be enhanced from 33.7% to 37.2% with a reduction in CM threshold from $3E_g$ to $2E_g$.[28] It might be possible for the CM threshold of $CuInSe_2$ to be further reduced. The minimum CM threshold of $CuInSe_2$ can be estimated based on the relationship[29]

$$E_{th} = \left(2 + \frac{m_e}{m_h}\right)E_g \quad (2)$$

where E_{th} is the CM threshold energy, and m_e and m_h are the electron and hole effective masses. Using bulk values for $CuInSe_2$ of $m_e = 0.1m_0$ and $m_h = 0.7m_0$, eq 2 give $E_{th} = 2.14E_g$, which is slightly lower than the measured value of $2.4E_g$.

$CuInSe_2$ nanocrystals can be made with a near optimal band gap in the range of 0.75−1.15 eV while simultaneously achieving long biexciton lifetimes, both of which depend on nanocrystal size.[26,28] The Auger lifetime is important for multiexciton extraction in solar cells, as the biexciton lifetime relates to the ability to extract the generated multiexcitons.[30] From the perspective of carrier extraction in a multiexciton solar cell, large nanocrystals with slow Auger decay rates would be used to minimize biexciton annihilation. At the same time, the benefit of slow Auger decay must be balanced with the need for increased band gap through quantum confinement. Detailed energy balances have shown that for an CM efficiency of 100% and a CM threshold of $2E_g$, the peak optimal nanocrystal band gap is near ~0.9 eV.[10,28,31] To achieve this near-optimum band gap from small band gap materials like PbS (0.5 eV) and PbSe (0.37 eV), relatively small nanocrystals are needed. Larger band gap semiconductors like $CuInSe_2$ (~1 eV) do not require significant quantum confinement and, therefore, can make use of nanocrystals with slower Auger decay that still exhibit relatively high CM efficiency. For $CuInSe_2$, the largest nanocrystals measured (9.2 nm diameter) have a near optimal band gap of 1.06 eV and a biexciton lifetime of 130 ps. PbSe has a bulk band gap of 0.37 eV, and particles must be confined to a diameter of 5−6 nm to achieve a band gap near 0.75 eV.[32,33] At

dx.doi.org/10.1021/jz501640f | J. Phys. Chem. Lett. 2014, 5, 3169−3174

these sizes, PbSe has a biexciton lifetime of ~30 ps.[34] The relevant biexciton lifetime for $CuInSe_2$ is, therefore, much longer than for PbSe.

In summary, TAS measurements showed that the CM efficiency of $CuInSe_2$ nanocrystals is comparable to other types of nanocrystals. The CM threshold of the nanocrystals in the size range studied was slightly higher ($2.4E_g$) than the value predicted by the carrier effective mass (of $2.14E_g$). A lower CM threshold closer to $2E_g$ and higher CM efficiency would improve the efficiency of multexciton solar cells. Nonetheless, the biexciton lifetimes are relatively long in the $CuInSe_2$ nanocrystals in this size range, which could aid in extracting multiexcitons from a solar cell. For these reasons, $CuInSe_2$ looks to be an interesting, and perhaps reasonably unique, material for the study and fabrication of multiexciton solar cells.

■ ASSOCIATED CONTENT

Supporting Information

Experimental details, UV−vis absorbance, X-ray diffraction, biexciton lifetime data fits, and data for calculating CM quantum yield. This material is available free of charge via the Internet at http://pubs.acs.org.

■ AUTHOR INFORMATION

Corresponding Author

*E-mail: korgel@che.utexas.edu. Tel.: +1-512-471-5633. Fax: +1-512-471-7060.

Notes

The authors declare no competing financial interest.

■ ACKNOWLEDGMENTS

Financial support of this work was provided by the Robert A. Welch Foundation (F-1464) and the National Science Foundation Industry/University Cooperative Research Center on Next Generation Photovoltaics (IIP-1134849). Financial support was also provided for C.J.S. by the National Science Foundation Graduate Research Fellowship Program under Grant No. DGE-11100007. Use of the Center for Nanoscale Materials was supported by the U. S. Department of Energy, Office of Science, Office of Basic Energy Sciences, under Contract No. DE-AC02-06CH11357.

■ REFERENCES

(1) Beard, M. C.; Midgett, A. G.; Hanna, M. C.; Luther, J. M.; Hughes, B. K.; Nozik, A. J. Comparing Multiple Exciton Generation in Quantum Dots To Impact Ionization in Bulk Semiconductors: Implications for Enhancement of Solar Energy Conversion. *Nano Lett.* **2010**, *10*, 3019−3027.

(2) Midgett, A. G.; Luther, J. M.; Stewart, J. T.; Smith, D. K.; Padilha, L. A.; Klimov, V. I.; Nozik, A. J.; Beard, M. C. Size and Composition Dependent Multiple Exciton Generation Efficiency in PbS, PbSe, and PbS_xSe_{1-x} Alloyed Quantum Dots. *Nano Lett.* **2013**, *13*, 3078−3085.

(3) Nootz, G.; Padilha, L. A.; Levina, L.; Sukhovatkin, V.; Webster, S.; Brzozowski, L.; Sargent, E. H.; Hagan, D. J.; Van Stryland, E. W. Size Dependence of Carrier Dynamics and Carrier Multiplication in PbS Quantum Dots. *Phys. Rev. B* **2011**, *83*, 155302.

(4) Beard, M. C.; Midgett, A. G.; Hanna, M. C.; Luther, J. M.; Hughes, B. K.; Nozik, A. J. Comparing Multiple Exciton Generation in Quantum Dots To Impact Ionization in Bulk Semiconductors: Implications for Enhancement of Solar Energy Conversion. *Nano Lett.* **2010**, *10*, 3019−3027.

(5) Schaller, R. D.; Agranovich, V. M.; Klimov, V. I. High-Efficiency Carrier Multiplication through Direct Photogeneration of Multi-Excitons via Virtual Single-Exciton States. *Nat. Phys.* **2005**, *1*, 189−194.

(6) Franceschetti, A.; An, J. M.; Zunger, A. Impact Ionization Can Explain Carrier Multiplication in PbSe Quantum Dots. *Nano Lett.* **2006**, *6*, 2191−2195.

(7) Allan, G.; Delerue, C. Influence of Electronic Structure and Multiexciton Spectral Density on Multiple-Exciton Generation in Semiconductor Nanocrystals: Tight-Binding Calculations. *Phys. Rev. B* **2008**, *77*, 125340.

(8) Velizhanin, K. A.; Piryatinski, A. Numerical Study of Carrier Multiplication Pathways in Photoexcited Nanocrystal and Bulk Forms of PbSe. *Phys. Rev. Lett.* **2011**, *106*, 207401.

(9) Beard, M. C.; Knutsen, K. P.; Yu, P.; Luther, J. M.; Song, Q.; Metzger, W. K.; Ellingson, R. J.; Nozik, A. J. Multiple Exciton Generation in Colloidal Silicon Nanocrystals. *Nano Lett.* **2007**, *7*, 2506−2512.

(10) Schaller, R. D.; Klimov, V. I. High Efficiency Carrier Multiplication in PbSe Nanocrystals: Implications for Solar Energy Conversion. *Phys. Rev. Lett.* **2004**, *92*, 186601.

(11) Ellingson, R. J.; Beard, M. C.; Johnson, J. C.; Yu, P.; Micic, O. I.; Nozik, A. J.; Shabaev, A.; Efros, A. L. Highly Efficient Multiple Exciton Generation in Colloidal PbSe and PbS Quantum Dots. *Nano Lett.* **2005**, *5*, 865−871.

(12) Lin, Z.; Franceschetti, A.; Lusk, M. T. Size Dependence of the Multiple Exciton Generation Rate in CdSe Quantum Dots. *ACS Nano* **2011**, *5*, 2503−2511.

(13) Sun, J.; Yu, W.; Usman, A.; Isimjan, T. T.; DGobbo, S.; Alarousu, E.; Takanabe, K.; Mohammed, O. F. Generation of Multiple Excitons in Ag_2S Quantum Dots: Single High-Energy versus Multiple-Photon Excitation. *J. Phys. Chem. Lett.* **2014**, *5*, 659−665.

(14) Stubbs, S. K.; Hardman, S. J. O.; Graham, D. M.; Spencer, B. F.; Flavell, W. R.; Glarvey, P.; Masala, O.; Pickett, N. L.; Binks, D. J. Efficient Carrier Multiplication in InP Nanoparticles. *Phys. Rev. B* **2010**, *81*, 081303.

(15) Califano, M. Direct and Inverse Auger Processes in InAs Nanocrystals: Can the Decay Signature of a Trion Be Mistaken for Carrier Multiplication? *ACS Nano* **2009**, *3*, 2706−2714.

(16) Luther, J. M.; Beard, M. C.; Song, Q.; Law, M.; Ellingson, R. J.; Nozik, A. J. Multiple Exciton Generation in Films of Electronically Coupled PbSe Quantum Dots. *Nano Lett.* **2007**, *7*, 1779−1784.

(17) Stolle, C. J.; Harvey, T. B.; Pernik, D. R.; Hibbert, J. I.; Du, J.; Rhee, D. J.; Akhavan, V. A.; Schaller, R. D.; Korgel, B. A. Multiexciton Solar Cells of $CuInSe_2$ Nanocrystals. *J. Phys. Chem. Lett.* **2014**, *5*, 304−309.

(18) Semonin, O. E.; Luther, J. M.; Choi, S.; Chen, H.-Y.; Gao, J.; Nozik, A. J.; Beard, M. C. Peak External Photocurrent Quantum Efficiency Exceeding 100% via MEG in a Quantum Dot Solar Cell. *Science* **2011**, *334*, 1530−1533.

(19) Panthani, M. G.; Stolle, C. J.; Reid, D. K.; Rhee, D. J.; Harvey, T. B.; Akhavan, V. A.; Yu, Y.; Korgel, B. A. $CuInSe_2$ Quantum Dot Solar Cells with High Open-Circuit Voltage. *J. Phys. Chem. Lett.* **2013**, *4*, 2030−2034.

(20) The band gap energy values estimated from optical absorption spectroscopy are different from those measured from TAS. For the purpose of calculations in this Letter, we used the band gap values measured from TAS.

(21) McGuire, J. A.; Sykora, M.; Joo, J.; Pietryga, J. M.; Klimov, V. I. Apparent Versus True Carrier Multiplication Yields in Semiconductor Nanocrystals. *Nano Lett.* **2010**, *10*, 2049−2057.

(22) Blackburn, J. L.; Ellingson, R. J.; Mićić, O. I.; Nozik, A. J. Electron Relaxation in Colloidal InP Quantum Dots with Photogenerated Excitons or Chemically Injected Electrons. *J. Phys. Chem. B* **2003**, *107*, 102−109.

(23) Yu, P.; Nedeljkovic, J. M.; Ahrenkiel, P. A.; Ellingson, R. J.; Nozik, A. J. Size Dependent Femtosecond Electron Cooling Dynamics in CdSe Quantum Rods. *Nano Lett.* **2004**, *4*, 1089−1092.

(24) Shabaev, A.; Efros, A. L.; Nozik, A. J. Multiexciton Generation by a Single Photon in Nanocrystals. *Nano Lett.* **2006**, *6*, 2856−2863.

(25) García-Santamaría, F.; Chen, Y.; Vela, J.; Schaller, R. D.; Hollingsworth, J. A.; Klimov, V. I. Suppressed Auger Recombination in "Giant" Nanocrystals Boosts Optical Gain Performance. *Nano Lett.* **2009**, *9*, 3482−3488.
(26) Beard, M. c.; Ellingson, R. j. Multiple Exciton Generation in Semiconductor Nanocrystals: Toward Efficient Solar Energy Conversion. *Laser Photonics Rev.* **2008**, *2*, 377−399.
(27) Midgett, A. G.; Hillhouse, H. W.; Hughes, B. K.; Nozik, A. J.; Beard, M. C. Flowing versus Static Conditions for Measuring Multiple Exciton Generation in PbSe Quantum Dots. *J. Phys. Chem. C* **2010**, *114*, 17486−17500.
(28) Hanna, M. C.; Nozik, A. J. Solar Conversion Efficiency of Photovoltaic and Photoelectrolysis Cells with Carrier Multiplication Absorbers. *J. Appl. Phys.* **2006**, *100*, 074510.
(29) Schaller, R. D.; Petruska, M. A.; Klimov, V. I. Effect of Electronic Structure on Carrier Multiplication Efficiency: Comparative Study of PbSe and CdSe Nanocrystals. *Appl. Phys. Lett.* **2005**, *87*, 253102.
(30) Trinh, M. T.; Limpens, R.; de Boer, W. D. A. M.; Schins, J. M.; Siebbeles, L. D. A.; Gregorkiewicz, T. Direct Generation of Multiple Excitons in Adjacent Silicon Nanocrystals Revealed by Induced Absorption. *Nat. Photonics* **2012**, *6*, 316−321.
(31) Klimov, V. I. Detailed-Balance Power Conversion Limits of Nanocrystal-Quantum-Dot Solar Cells in the Presence of Carrier Multiplication. *Appl. Phys. Lett.* **2006**, *89*, 123118.
(32) Moreels, I.; Lambert, K.; Smeets, D.; De Muynck, D.; Nollet, T.; Martins, J. C.; Vanhaecke, F.; Vantomme, A.; Delerue, C.; Allan, G.; et al. Size-Dependent Optical Properties of Colloidal PbS Quantum Dots. *ACS Nano* **2009**, *3*, 3023−3030.
(33) Moreels, I.; Lambert, K.; De Muynck, D.; Vanhaecke, F.; Poelman, D.; Martins, J. C.; Allan, G.; Hens, Z. Composition and Size-Dependent Extinction Coefficient of Colloidal PbSe Quantum Dots. *Chem. Mater.* **2007**, *19*, 6101−6106.
(34) Stewart, J. T.; Padilha, L. A.; Qazilbash, M. M.; Pietryga, J. M.; Midgett, A. G.; Luther, J. M.; Beard, M. C.; Nozik, A. J.; Klimov, V. I. Comparison of Carrier Multiplication Yields in PbS and PbSe Nanocrystals: The Role of Competing Energy-Loss Processes. *Nano Lett.* **2012**, *12*, 622−628.

■ NOTE ADDED AFTER ASAP PUBLICATION

This paper was published ASAP on September 3, 2014. Figure 6 was updated. The revised paper was reposted on September 4, 2014.